Subwavelength lithography over extended areas

Gunnar Björk* and Luis L. Sánchez-Soto
Departamento de Óptica, Facultad de Ciencias Físicas, Universidad Complutense, 28040 Madrid, Spain

Jonas Söderholm
Department of Electronics, Royal Institute of Technology (KTH), Electrum 229, SE-164 40 Kista, Sweden
(Received 24 January 2001; published 8 June 2001)

We demonstrate a systematic approach to subwavelength resolution lithographic image formation on films covering areas larger than a wavelength squared. For example, it is possible to make a lithographic pattern with a feature size resolution of $\lambda/[2(N+1)]$ by using a particular $2M$-photon, multimode entangled state, where $N \leqslant M$, and banks of birefringent plates. By preparing such a statistically mixed state, one can form any pixel pattern on a $2^{M-N}(N+1)\times 2^{M-N}(N+1)$ pixel grid occupying a square with side $L=2^{M-N-1}\lambda$. Hence, there is a trade off between the exposed area, the minimum lithographic feature size resolution, and the number of photons used for the exposure. We also show that the proposed method will work even under nonideal conditions, albeit with somewhat poorer performance.

DOI: 10.1103/PhysRevA.64.013811 PACS number(s): 42.50.Dv, 42.25.Hz, 42.65.−k, 85.40.Hp

I. INTRODUCTION

Classically, to create an optical image, one has to modulate a wave front of an electromagnetic wave in space. The minimum resolvable feature size of an imaged object corresponds, roughly speaking, to the minimum modulation period allowed, which turns to be of the order of the wavelength λ of the light used. In fact, the best resolution that can be achieved classically is about $\lambda/2$, which is usually known as the diffraction limit.

When the quantum nature of light is considered, one is naturally confronted with the role that photon fluctuations play in setting fundamental performance limits for imaging systems. Even if all the *technical* noise sources are eliminated from the imaging system, the corpuscular nature of the photon induces fluctuations, or shot noise, that determine a seemingly fundamental spatial resolution, or standard quantum limit, of about $\lambda/(2\sqrt{N})$, where N is the average number of photons. Subwavelength imaging has been used in a number of applications [1–6] and a careful analysis shows that indeed the shot noise sets the resolution limit [5,6].

However, the quantum viewpoint allows for strategies that could significantly improve the spatial resolution beyond the standard quantum limit. A typical way of reducing photon-counting noise is by using multimode squeezed light [7–12]. This possibility has been experimentally demonstrated in other precision measurement schemes [13] and allows one to attain an optimum spatial resolution proportional to $\lambda/(2N)$, usually known as the Heisenberg limit. These sub shot-noise imaging systems enable resolving, in principle, arbitrarily small details of an object in a diffraction-limited optical system.

However, writing images imposes even more stringent requirements than subwavelength resolution of spatial features, because in image writing one wants to write small details with *high contrast*. A particular field where circumventing the classical resolution limit is becoming more and more important is optical lithography, which is the primary tool for writing electronic-circuit patterns. Current production technologies have tended to use light of shorter wavelengths to fabricate ever-smaller device features.

It has been known for some time that entangled photon pairs can be used to achieve Heisenberg-limited resolution of time [14–16] and phase [17–20], but only very recently has the use of entanglement to increase high-contrast image resolution indefinitely [21–24] been proposed. The reason that these entangled quantum states show increased resolution can be traced back to the fact that they allow the modulation period to be as small as $\lambda/(2N)$, and thus, they approach Heisenberg-limited resolution. The process can be envisioned as the photons clustering into a N-photon quasiparticle with a linear momentum N times as large as that of a single photon, and therefore with a shorter de Broglie wavelength [25]. It is the de Broglie wavelength that ultimately determines the interference resolution. This has been appreciated for a long time in atomic, molecular, and solid-state physics, but has only recently been noticed for electromagnetic waves.

In an earlier paper, we discussed the use of reciprocal binomial states in subwavelength resolution lithography [24]. Our method works for even number of photons $2N$ and it is especially germane to determine the exposure sequence to generate any pixellated pattern on a $(N+1)\times(N+1)$ grid, occupying a square with a half wavelength long side. An advantage with the method is that only one particular entangled state needs to be generated: all other necessary states can be produced from the first by means of, e.g., a small bank of phase plates with a prescribed birefringence. Unfortunately, it is not possible to generate larger patterns since the deposition methods proposed hitherto all are periodic with a period of half a wavelength [21–24]. Restricting the exposure source of the lithography to four modes, with pair-

*On leave from Department of Electronics, Royal Institute of Technology (KTH), Electrum 229, SE-164 40 Kista, Sweden; electronic address: gunnarb@ele.kth.se; URL: http://www.ele.kth.se/QEO/

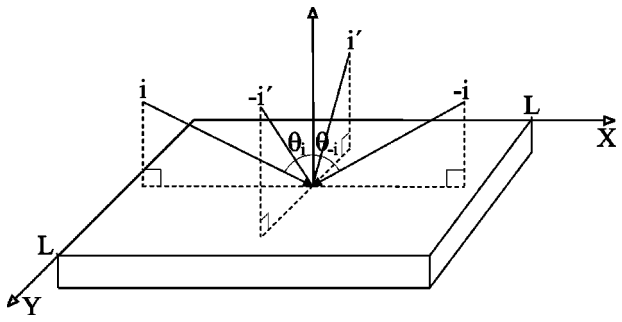

FIG. 1. A schematic showing the geometry of the lithographic exposure.

wise opposite wave vectors (Fig. 1) one can only increase the size of the pattern by some factor by sacrificing the pattern resolution by exactly the same factor. To be able to adjust the size of the deposited pattern *independently* of the resolution, one must use more modes. In this paper, we report a systematic multimode extension to the method we proposed earlier [24].

II. SUBWAVELENGTH LITHOGRAPHY

A. One dimension, two modes

Our goal is to establish how to create arbitrary two-dimensional patterns on a squared substrate of side L. Suppose we have two counter-propagating beams in a direction we shall denote X, see Fig. 1. The beams propagate at angles $\pm\theta$ to the normal of the substrate. This substrate is coated with lithographic resist (in the following, we will refer to the resist as the film) and situated in the region where the beams overlap. In general, provided the coherence lengths of the wave packets are much longer than the side of the film, we do not need to take into account the mode shapes and we will assume that they are plane over the side of the film.

Following Ref. [21], the lithographic film absorption is modeled by an M-photon absorption process. Thus, the absorption process can be modeled by the operator $\hat{e}^{\dagger M}\hat{e}^{M}$ given by

$$\hat{e}^{\dagger M}\hat{e}^{M}=\left(\frac{1}{\sqrt{W}}\sum_{i}\hat{a}_{i}^{\dagger}\right)^{M}\left(\frac{1}{\sqrt{W}}\sum_{i}\hat{a}_{i}\right)^{M}, \tag{2.1}$$

where $\hat{a}_i$ is the annihilation operator of mode i, and W is the number of excited modes impinging on the film. In this way, higher-order interference effects are naturally brought out. The photosensitive ''grains'' in the film must be much smaller than the shortest de Broglie wavelength encountered in the exposure process. Therefore, from the point of view of a ''grain,'' the photon packets in the respective modes will be indistinguishable in spite of their different linear momenta, as manifested by Eq. (2.1).

Let us now discuss the interference in one dimension between a pair of modes, labeled -1 and 1, propagating in the plane defined by the X axis and the film normal. We restrict ourselves to consider states that are eigenstates N_1 of the total photon number in the modes ± 1. According to our assumptions, the deposition rate in the substrate Δ_M is proportional to the expectation value of the operator $\hat{e}^{\dagger M}\hat{e}^{M}$, where $\hat{e}=(\hat{a}_{-1}+\hat{a}_1)/\sqrt{2}$. Let us further assume that the two beams impinge at the angles $\theta_{\pm 1}=\pm\pi/2$. The beams will hence strike the film surface at grazing incidence. Furthermore, we shall assume that the modes are prepared in a two-mode reciprocal binomial state of the general form

$$|\psi^{(N_i)}\rangle=\frac{1}{\sqrt{\mathcal{N}_i}}\sum_{n=0}^{N_i}\sqrt{n!(N_i-n)!}|n\rangle_i\otimes|N_i-n\rangle_{-i}, \tag{2.2}$$

where N_i is the total photon number of the two modes and $\mathcal{N}_i=\Sigma_{n=0}^{N_i}n!(N_i-n)!$ is a normalization factor.

Let the X coordinate normalized to the optical wavelength λ be denoted x. Since the two modes -1 and 1 impinge over the film in antiparallel directions, the accumulated phase of mode 1 (propagating in the positive X direction) at a distance λx from the left edge of the film will be

$$\mathcal{U}_1=\exp(ik\lambda x\hat{a}_1^{\dagger}\hat{a}_1)=\exp(i2\pi x\hat{a}_1^{\dagger}\hat{a}_1), \tag{2.3}$$

where $k=2\pi/\lambda$, while mode -1 will have accumulated the phase

$$\mathcal{U}_{-1}=\exp[ik\lambda(1-x)\hat{a}_{-1}^{\dagger}\hat{a}_{-1}]=\exp[i2\pi(1-x)\hat{a}_{-1}^{\dagger}\hat{a}_{-1}] \tag{2.4}$$

at the same location. Using these free-space unitary propagation operators, we find that at the location x, the state (2.2) for modes ± 1 is transformed into

$$|\psi_x^{(N_1)}\rangle=\frac{1}{\sqrt{\mathcal{N}_1}}\sum_{n=0}^{N_1}e^{i2\pi x(2n-N_1)}\times\sqrt{n!(N_1-n)!}|n\rangle_1\otimes|N_1-n\rangle_{-1}. \tag{2.5}$$

We can now translate the substrate a distance $\lambda/[4(N_1+1)]$ to the left, and at the same time, phase shift mode 1 by $2\pi\ell_{1x}/(N_1+1)$ ($\ell_{1x}=1,2,\ldots,N_1+1$) relative to mode -1. The corresponding state will be labeled $|\psi_x^{(N_1,\ell_{1x})}\rangle$, where

$$|\psi_x^{(N_1,\ell_{1x})}\rangle=\frac{1}{\sqrt{\mathcal{N}_1}}\sum_{n=0}^{N_1}e^{i\pi[2x-(\ell_{1x}-1/2)/(N_1+1)](2n-N_1)}\times\sqrt{n!(N_1-n)!}|n\rangle_1\otimes|N_1-n\rangle_{-1}. \tag{2.6}$$

As shown in Ref. [24], this state will deposit a ''one-dimensional pixel,'' that is, the deposition rate Δ_M will have a single pronounced peak $\lambda/[2(N_1+1)]$ wide, occupying the interval on the X axis between $\lambda(\ell_{1x}-1)/[2(N_1+1)]$ and $\lambda\ell_{1x}/[2(N_1+1)]$.

To make a qualitative comparison between the subwavelength resolution lithographic method proposed in Refs. [21,23] and our method, we have calculated the deposition pattern when the target pattern is a rectangular trench. In Refs. [21,23] such a trench, $\lambda/4$ wide, was used as a trial

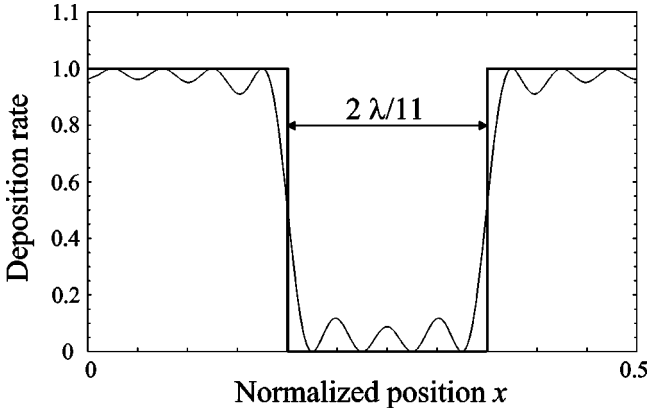

FIG. 2. The deposition rate due to a pair of modes with $\theta_{\pm 1} = \pm \pi/2$ and $N=10$ in an equal statistical mixture state between $|\psi_x^{(10,1)}\rangle$, $|\psi_x^{(10,2)}\rangle$, $|\psi_x^{(10,3)}\rangle$, $|\psi_x^{(10,4)}\rangle$, $|\psi_x^{(10,9)}\rangle$, $|\psi_x^{(10,10)}\rangle$, and $|\psi_x^{(10,11)}\rangle$. A trench, four pixels wide ($=4\lambda/22$) is formed. The unwanted exposure modulation of both the exposed and the unexposed pixels is on the order of 10% of the maximum exposure. The target deposition function is drawn with thick lines.

target function for a 10-photon state. We have done the same, but since a 10-photon state will define an 11-pixel pattern (in one dimension) the natural target trench function in our case is an integer number of pixels wide. The pixel width for a 10-photon state is $\lambda/22$. In Fig. 2 we have calculated the deposition rate for a four-pixel wide trench, that is, a trench $2\lambda/11 \approx 0.18\lambda$ wide. In order to make this pattern we can, e.g., expose the pixels sequentially employing the states indicated in the figure caption. Although not shown in the figure, remember that this two-mode deposition rate is periodic with the period $\lambda/2$.

We see that the result of our method is almost the same, both in the respect of edge sharpness and in exposure penalty, to those obtained by the method proposed by Boto *et al.* [21,23]. As we shall show below, neither the edge sharpness nor the exposure penalty need to be sacrificed when the lithographic pattern is extended over areas larger than half a wavelength in each dimension. A fundamental difference between the methods is that the pattern-producing state is pure in the proposal of Boto *et al.*, while our proposal is based on mixed states (or a sequence of pure states if each pixel is deposited separately).

B. One dimension, four modes

To overcome the limiting $\lambda/2$ periodicity of the deposition rate, we introduce another pair of modes -2 and 2 impinging along the X direction at angles $\theta_{\pm 2} = \pm \arcsin[1/(N_2+1)]$ from the film normal. Hence, they have only the wave vector components $\pm 2\pi/[\lambda(N_2+1)]$ in the X direction. We assume that this pair of modes are prepared in a reciprocal binomial state, too. Consequently, their state at location x is given by

$$|\phi_x^{(N_2)}\rangle = \frac{1}{\sqrt{\mathcal{N}_2}} \sum_{n=0}^{N_2} e^{i2\pi x(2n-N_2)/(N_2+1)} \times \sqrt{n!(N_2-n)!}\,|n\rangle_2 \otimes |N_2-n\rangle_{-2}. \quad (2.7)$$

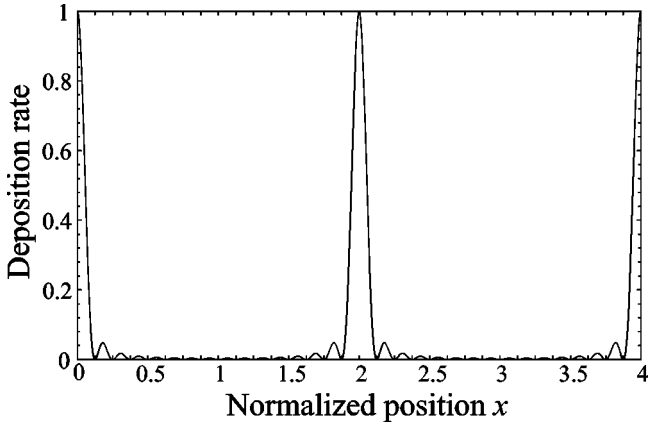

FIG. 3. The deposition rate due to two pairs of modes with $\theta_{\pm 1} = \pm \pi/2$ and $\theta_{\pm 2} = \pm \arcsin(1/4)$ that are prepared in two three-photon reciprocal binomial states. The deposition rate is periodic with period 2λ. The width of the deposition rate peak is roughly $\lambda/8$.

(We use the symbol ϕ in the ket above to indicate that the modes corresponding to the state do not impinge at grazing incidence over the film surface.)

Now suppose the (N_1+N_2)-photon, product state $|\psi_x^{(N_1)}\rangle \otimes |\phi_x^{(N_2)}\rangle$ is prepared. Calculating the pattern deposition rate Δ_M, where now $\hat{e} = (\hat{a}_{-2} + \hat{a}_{-1} + \hat{a}_1 + \hat{a}_2)/2$ and $M = N_1 + N_2$, we find that

$$\Delta_M \propto \left| \sum_{m=0}^{N_1} e^{i2\pi x(2m-N_1)} \sum_{n=0}^{N_2} e^{i2\pi x(2n-N_2)/(N_2+1)} \right|^2 \propto \frac{1}{[(N_1+1)(N_2+1)]^2} \frac{\sin^2[2(N_1+1)\pi x]}{\sin^2[2\pi x/(N_2+1)]}. \quad (2.8)$$

The deposition rate Δ_M has a highest oscillation period in x of $1/[2(N_1+1)]$ and an overall periodicity of $(N_2+1)/2$, corresponding to the physical lengths $\lambda/[2(N_1+1)]$ and $\lambda(N_2+1)/2$, respectively. A plot of Eq. (2.8) for the case $N_1 = N_2 = 3$ is shown in Fig. 3. Note that the deposition-function spatial resolution is $\lambda/8$ and its periodicity is 2λ.

When we translate the substrate a distance $\lambda/[4(N_1+1)]$ to the left, and at the same time, phase shift mode 2 by $2\pi \ell_{2x}/(N_2+1) + 2\pi \ell_{1x}/[(N_1+1)(N_2+1)]$ ($\ell_{2x} = 1,2,\ldots,N_2+1$) relative to mode -2, the state $|\phi_x^{(N_2)}\rangle$ in modes ± 2 is transformed to

$$|\phi_x^{(N_2,\ell_{1x},\ell_{2x})}\rangle = \frac{1}{\sqrt{\mathcal{N}_2}} \sum_{n=0}^{N_2} e^{i\pi[2x - \ell_{2x} - (\ell_{1x}-1/2)/(N_1+1)](2n-N_2)/(N_2+1)} \times \sqrt{n!(N_2-n)!}\,|n\rangle_2 \otimes |N_2-n\rangle_{-2}. \quad (2.9)$$

Using Eqs. (2.6) and (2.9) we see that the four-mode state $|\psi_x^{(N_1)}\rangle \otimes |\phi_x^{(N_2)}\rangle$ will consequently be transformed into the state $|\psi_x^{(N_1,\ell_{1x})}\rangle \otimes |\phi_x^{(N_2,\ell_{1x},\ell_{2x})}\rangle$ after the translation and re-

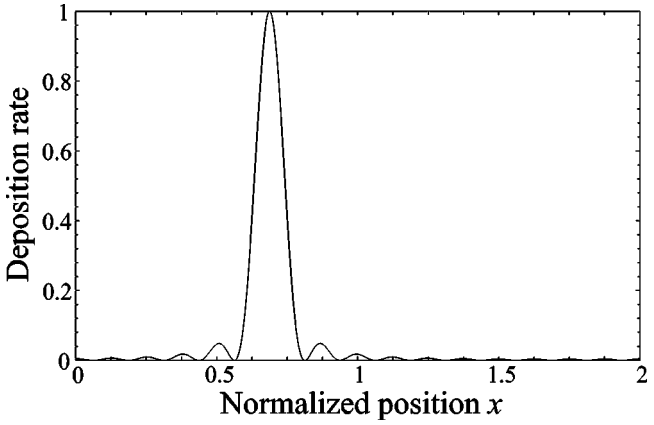

FIG. 4. The deposition rate due to two pairs of modes with $\theta_{\pm 1}=\pm\pi/2$ and $\theta_{\pm 2}=\pm$ arcsin (1/4) in the six-photon reciprocal binomial product state $|\psi_x^{(3,2)}\rangle\otimes|\phi_x^{(3,2,1)}\rangle$ exposing pixel number six. The deposition rate is periodic with period 2λ. Only one period is shown.

spective relative phase shifts. The deposition rate for this state can readily be calculated to be

$$\Delta_M(\ell_{1x},\ell_{2x})\propto\frac{1}{[(N_1+1)(N_2+1)]^2}\times\frac{\sin^2\{[2(N_1+1)x-\ell_{1x}+1/2]\pi\}}{\sin^2\left[\left(2x-\ell_{2x}-\frac{\ell_{1x}-1/2}{N_1+1}\right)\frac{\pi}{N_2+1}\right]}. \tag{2.10}$$

If we divide the part of the X axis between the origin and the point $x=(N_2+1)/2$ into $(N_1+1)(N_2+1)$ pieces, each $1/[2(N_1+1)]$ long, each interval will represent a ''one-dimensional pixel.'' With a specific choice of ℓ_{1x} and ℓ_{2x} we can deposit (or expose) pixel number $\ell_{1x}+(N+1)\ell_{2x}$ [numbered from left to right and the number taken modulo $(N_1+1)(N_2+1)$] with a negligible exposure penalty (that is, negligible unwanted exposure of nominally unexposed pixels). This can be clearly seen in Fig. 4, where we have assumed that $N_1=N_2=3$, $\ell_{1x}=2$, and $\ell_{2x}=1$, leading to the exposure of pixel number 6. The relative phase-shifts between the modes, labeled by the numbers ℓ_{1x} and ℓ_{2x}, can be accomplished via a bank of appropriately chosen birefringent plates, provided that the modes ± 1 and ± 2, respectively, are originally prepared in spatially and temporally degenerate modes, but with orthogonal polarizations, as discussed in Ref. [24].

The deposition-rate function (2.10) has two special properties that are worth pointing out. The first is that the deposition rate will be identically zero at the center of all unexposed pixels regardless of what other pixels are exposed. Hence, a nominally unexposed pixel surrounded by exposed pixels will remain unexposed at the pixel center. This is a very appealing feature of the proposed method since the exposure penalty hardly depends at all on the particular pixel pattern one intends to expose. The second nice feature is that the sum of the deposition-rate functions for all pixels add up to unity; i.e.,

$$\sum_{\ell_{1x}=1}^{N_1+1}\sum_{\ell_{2x}=1}^{N_2+1}\Delta_M(\ell_{1x},\ell_{2x})\equiv 1, \tag{2.11}$$

for all values of x. This, in turn, means that we never risk overexposure, even if we expose two or more adjacent pixels. In fact, if a row, or column, of adjacent pixels are exposed, the resulting deposition function ridge will hardly have any modulation [24]. The identity (2.11) also means that if one wants to make the negative image of some pixel pattern, one can construct *identically* the negative image deposition rate by exposing all previously unexposed pixels, and vice versa.

Let us now discuss the geometrical scaling properties of the deposition rate. By decreasing the modes' wave-vector components in the film plane by a fixed factor, both the minimum feature-size resolution and the fundamental period of deposition rate will increase by the same factor. If we, e.g., let modes ± 1 impinge at angles $\pm$ arcsin(1/2) from the film normal and modes ± 2 impinge at the angles $\pm$ arcsin$(1/[2(N_2+1)])$, then the minimum feature size resolution (i.e., pixel size) becomes $\lambda/(N_1+1)$ and the period of the deposition rate becomes $(N_2+1)\lambda$. However, the wave-vector component parallel to the film is not only governed by the modes' propagation angles, but it is also governed by the de Broglie wavelength of the impinging states. Therefore, the pixel and pattern sizes are intimately connected to how we prepare the states. If the (one-dimensional) film is modeled as a $M=2N$-photon absorber, the choice to partition the $2N$ photons equally between the two pairs of modes ± 1, and ± 2, as assumed in Fig. 4, is by no means necessary. Instead we can, e.g., prepare modes -1 and 1 in a two-mode $(N-1)$-photon state $|\psi_x^{(N-1)}\rangle$ and the modes -2 and 2 in a two-mode $(N+1)$-photon state $|\phi_x^{(N+1)}\rangle$. The appropriate relative phase shifts are $2\pi\ell_{1x}/N$, where $\ell_{1x}=1,2,\ldots,N$ and $2\pi\ell_{2x}/(N+2)+2\pi\ell_{1x}/(N^2+2N)$ where $\ell_{2x}=1,2,\ldots,N+2$, respectively. In this case, the minimum lithographic feature size resolution becomes $\lambda/(2N)$, the number of individually depositable pixels become $N(N+2)$, and the fundamental period of the deposition rate becomes $\lambda(N+2)/2$. An illustration of an ensuing deposition rate function is given in Fig. 5. Continuing this repartition, one can either increase the fundamental period of the deposition rate at the expense of increasing the minimum resolution by increasing the photon number in modes ± 2 at the expense of the photon number in modes ± 1, or vice versa. The attainable minimum size resolution and deposition rate period are shown in Table I.

C. Two dimensions, eight modes

One can now extend the lithographic exposure procedure to two dimensions by simply introducing two additional pairs of modes $\pm 1'$ and $\pm 2'$, impinging towards the film at corresponding angles to modes ± 1 and ± 2, but in the Y direction, perpendicular to X [24]. If the eight modes are

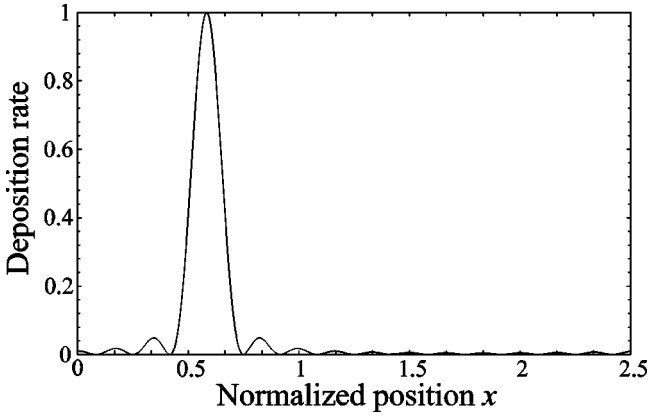

FIG. 5. The deposition rate due to two pairs of modes with $\theta_{\pm 1}=\pm\pi/2$ and $\theta_{\pm 2}=\pm$ arcsin (1/5) in the state $|\psi_x^{(2,1)}\rangle \otimes |\phi_x^{(4,1,1)}\rangle$. In comparison to the example in Fig. 4, the pixel size is increased by a factor 4/3 to $\lambda/6$, while the deposition-rate period has increased by a factor 5/4 to $5\lambda/2$.

prepared in the initial state $|\psi_x^{(N,\ell_{1x})}\rangle \otimes |\phi_x^{(N,\ell_{1x},\ell_{2x})}\rangle \otimes |\psi_y^{(N,\ell_{1y})}\rangle \otimes |\phi_y^{(N,\ell_{1y},\ell_{2y})}\rangle$, the deposition rate is given by the product of the corresponding deposition rates in the X and in the Y direction. Of course, if the number of photons in each of the two-mode states $|\psi_x^{(N,\ell_{1x})}\rangle, \ldots, |\phi_y^{(N,\ell_{1y},\ell_{2y})}\rangle$ is N, then the film must have a non-negligible $M=4N$-photon absorption cross section. If so, the assumed state will expose the pixel $(\ell_{1x}+(N+1)\ell_{2x}, \ell_{1y}+(N+1)\ell_{2y})$ and leave the remaining pixels essentially unexposed. In order to expose a pattern, such as a line of adjacent pixels, one must prepare a statistical mixture of the pixels' associated states, or one can expose the pixels sequentially. As shown in Ref. [24], diagonal lines composed of exposed pixels will have an unacceptably large deposition-rate fluctuation along the diagonal center line. However, the minima can be ''filled in'' by depositing intermediate pixels (with their centers at the intersection points between four adjacent regular pixels). Again, the states corresponding to these intermediate pixels can be prepared by appropriate relative phase shifts between the mode pairs [24]. For the rest of this paper, we shall only study the deposition rates in one dimension, bearing in mind that with our method, the two-dimensional deposition-rate function is simply the product of two one-dimensional functions.

III. GENERALIZED MULTIMODE QUANTUM LITHOGRAPHY

It is clear that the procedure to increase the deposition-rate period is not limited by considering only two pairs of modes with opposite wave vectors in each dimension. We can continue this procedure by introducing a third pair of modes, labeled -3 and 3, impinging towards the film at the angles $\theta_{\pm 3}=\pm$ arcsin$[1/(N+1)^2]$ from the film normal. If the number of photons M contributing to the film absorption process is divisible by 3 (or 6, in two dimensions), so that $M=3N$, and this photon number is partitioned equally between the three modes, then one will be able to deposit any pixellated patterns with the minimum feature-size resolution of $\lambda/[2(N+1)]$ over a length of $L=\lambda(N+1)^2/2$.

However, in order to cover the maximum area for a given number of photons M and resolvable feature size $\lambda/[2(N+1)]$, where $1\leqslant N<M$, the following product state should be prepared:

$$|\psi_x^{(N,\ell_{1x})}\rangle \otimes |\phi_x^{(1,\ell_{1x},\ell_{2x})}\rangle \otimes \ldots \otimes |\phi_x^{(1,\ell_{1x},\ell_{2x},\ldots,\ell_{(M-N)x})}\rangle, \tag{3.1}$$

where $\ell_{1x}=1,2,\ldots,N+1$, $\ell_{2x},\ldots,\ell_{(M-N)x}=1,2$, and modes ± 1 impinge at grazing incidence, while modes $\pm i$, $i=2,\ldots,M-N$, impinge at the angles $\theta_{\pm i}=\pm$ arcsin$[2^{-(i-1)}]$. The rationale for preparing this state is that the state $|\psi_x^{(N,\ell_{1x})}\rangle$ will determine the feature size resolution and will let us deposit any one of $N+1$ pixels each with a size of $\lambda/[2(N+1)]$. With the remaining $M-N$ photons, each of the one photon states $|\phi_x^{(1,\ell_{1x},\ell_{2x})}\rangle, \ldots, |\phi_x^{(1,\ell_{1x},\ell_{2x},\ldots,\ell_{(M-N)x})}\rangle$ will allow us to double the fundamental period of the deposition-rate function. If we compare this to a case where the $M-N$ photons are partitioned between a smaller number of more highly excited states, it is clear that the state (3.1) gives a longer fundamental deposition-rate period since $2^{M-N}\geqslant M-N+1$ for all relevant numbers M and N. With the initial state (3.1) one will be able to deposit any one of $2^{M-N}(N+1)$ pixels in one dimension, where each pixel is $\lambda/[2(N+1)]$ wide. The fundamental period of the pixel pattern will be $L=2^{M-N-1}\lambda$. With $2M$ photons one will be able to make a two-dimensional pattern with this resolution and periodicity in both dimensions. This is the major result in this paper. In

TABLE I. A table demonstrating the number of depositable pixels, minimum feature size resolution, and the fundamental deposition rate periodicity for different partitions of $N_1+N_2=2N$ photons between two pairs of modes in one dimension.

N_1	N_2	Number of pixels	Feature size	Periodicity
$2N$	0	$2N+1$	$\lambda/(4N+2)$	$\lambda/2$
$2N-1$	1	$4N$	$\lambda/4N$	λ
$\vdots$	$\vdots$	$\vdots$	$\vdots$	$\vdots$
n	$2N-n$	$(n+1)(2N-n+1)$	$\lambda/2(n+1)$	$(2N-n+1)\lambda/2$
$\vdots$	$\vdots$	$\vdots$	$\vdots$	$\vdots$
1	$2N-1$	$4N$	$\lambda/4$	$N\lambda$
0	$2N$	$2N+1$	$\lambda/2$	$(2N+1)\lambda/2$

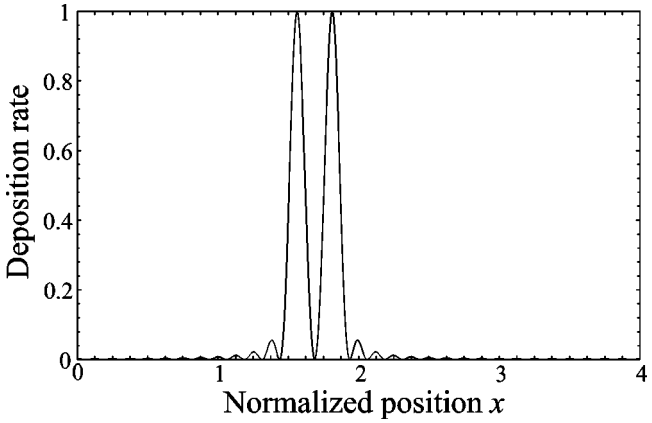

FIG. 6. The deposition rate due to a superposition state of four pairs of modes with three, one, one, and one photon. The pixel size is $\lambda/8$, while the deposition rate period has increased to 4λ. The relative phase shifts of the states have been chosen so that pixels 13 and 15 are exposed. As can be seen, the deposition rate is zero at the center of pixel 14.

Fig. 6, we have plotted the one-dimensional deposition rate from the interference between eight modes in a statistical mixture of the states

$$|\psi_x^{(3,1)}\rangle\otimes|\phi_x^{(1,1,1)}\rangle\otimes|\phi_x^{(1,1,1,1)}\rangle\otimes|\phi_x^{(1,1,1,1,0)}\rangle \qquad (3.2)$$

and

$$|\psi_x^{(3,3)}\rangle\otimes|\phi_x^{(1,3,1)}\rangle\otimes|\phi_x^{(1,3,1,1)}\rangle\otimes|\phi_x^{(1,3,1,1,0)}\rangle, \qquad (3.3)$$

where modes ± 1 impinge at $\theta_{\pm 1}=\pm\pi/2$ and the remaining three pairs of modes impinge at the angles $\theta_{\pm 2}=\pm\arcsin(1/2)$, $\theta_{\pm 3}=\arcsin(1/4)$, and $\theta_{\pm 4}=\pm\arcsin(1/8)$. The total photon number in all states is six, the same number assumed in Figs. 4 and 5. The ensuing 32-pixel pattern is the largest one-dimensional pattern one can make with six photons provided that the minimum feature size is fixed to $\lambda/8$. The price for the large number of depositable pixels is the difficulty one will have generating this eight-mode state. If the states' relative phase shifts are generated by birefringent phase plates, one will need two plates for the first pair of modes, and three, four, and five plates for the remaining three pairs of modes, respectively. We can, in principle, continue this process *ad infinitum*, but for a fixed minimum feature size, this requires M, the number of photons contributing to the exposure process, to increase. Since the absorption cross section quite generally decreases rapidly with increasing M, there will be a practical limit to such an extension.

IV. IMPERFECTIONS DUE TO LOSSES AND COMPETING MULTIPHOTON ABSORPTION PROCESSES

Above we have discussed how subwavelength imaging can work under ideal conditions. However, in order for the proposed method to be of practical use it is necessary that it is robust against imperfections. Below we shall discuss three mechanisms that will deteriorate the image forming ability of entangled states: linear losses, competing multiphoton absorption processes, and exposure noise due to light quantization.

First we will discuss the effect of losses occuring between the state generator and the film. As long as the film strictly absorbs the same number of photons as the generated multimode state contains, losses will not affect the lithographic resolution, it will only lower the deposition rate by a fixed amount. This is rather obvious, because if one or more photons are lost from an M-photon state, no M-photon absorption process can be triggered by the state. However, if there exists a competing $(M-1)$-photon absorption process in the film, the film may be exposed even after a photon is lost. In this case, the modified deposition rate will be the same whether the photon is lost before impinging on the film or if only $M-1$ out of M photons impinging on the film are absorbed. Losses prior to the film will, however, shift the relative proportion between $(M-1)$- and M-photon absorption processes in favor of the former by decreasing the probability that the state impinging on the film contains M photons. Therefore, losses in the optical system prior to the film should be kept as low as possible. Fortunately, losses will only gradually increase the required exposure dose and shift the probability of absorption toward absorption processes involving a smaller number of photons.

Next, we shall examine how the deposition rate of a M-photon state is affected by absorption processes involving less than M photons. Two physical effects will deteriorate the resolution and the exposure penalty in this case. One is that if the state contains M photons, but only $M-1$ of them are absorbed, there are as many final states as there are modes. If we look at the simplest case, an impinging two-mode state $|\psi_x^{(M)}\rangle$, the possible final states are $|1,0\rangle$ and $|0,1\rangle$. Since these states are distinguishable, the absorption probability amplitudes leading to one of these final states will not interfere with the amplitudes leading to the other. Only the initial state $|M,0\rangle$ ($|0,M\rangle$) will evolve into the state $|1,0\rangle$ ($|0,1\rangle$) with certainty upon absorption of $M-1$ photons. (All other number-difference states $|M-n,n\rangle$, $n\neq 0,M$ can evolve either into $|1,0\rangle$ or $|0,1\rangle$). This means that the two extreme number-difference states in the expansion of $|\phi_x^{(M)}\rangle$ cannot interfere at all in a $M-1$ photon absorption process. Therefore, the Fourier component with the highest spatial frequency will be absent in the ensuing deposition rate. Hence, the *spatial resolution* will decrease monotonically with decreasing order of the absorption process. A second effect will be that the destructive interference between the absorption probabilities outside the designated pixel will be incomplete, leading to an increased *exposure penalty*.

In Fig. 7 we have drawn the deposition rates of the state $|\psi_x^{(4,3)}\rangle$ due to four-, three-, two-, and one-photon absorption processes. The curves have been normalized such that the deposition rates all have a maximum of unity to facilitate comparisons. It can be seen that the width of the deposition-rate peak increases, and so does the exposure penalty as the mismatch between the state and the absorption process increases. It is, of course, possible to make a better deposition-rate function for, e.g., a three-photon absorption film by exposing the film by a state of the kind $|\psi_x^{(3)}\rangle$ instead of the

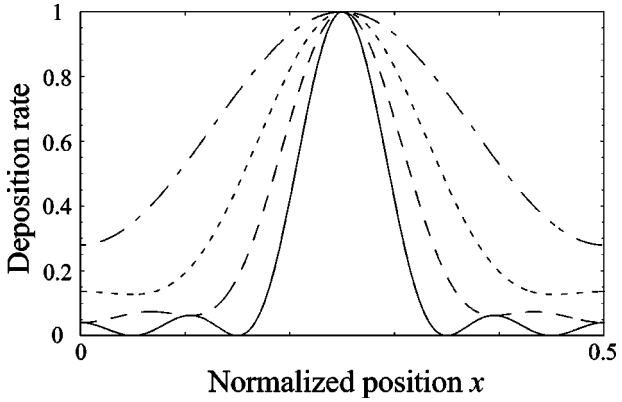

FIG. 7. The deposition rate due to a pair of modes with $\theta_{\pm 1} = \pm \pi/2$ in the state $|\psi_x^{(4,3)}\rangle$. The solid line shows the deposition rate for a four-photon absorption film. The dashed, dotted, and dash-dotted lines represent the (normalized) deposition rate for three-, two-, and one-photon absorption processes, respectively.

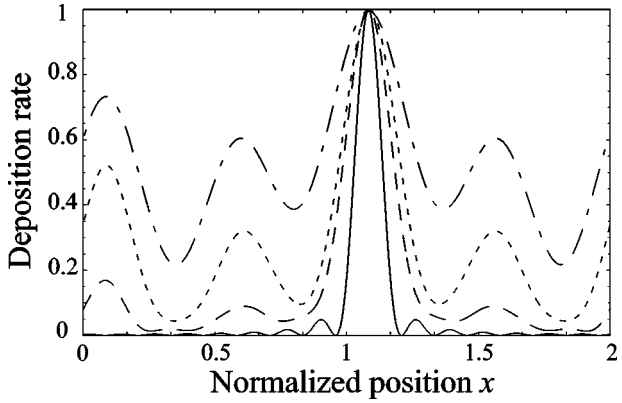

FIG. 8. The deposition rate due to three pairs of modes with $\theta_{\pm 1} = \pm \pi/2$, $\theta_{\pm 2} = \pm$ arcsin (1/2), and $\theta_{\pm 3} = \pm$ arcsin (1/4) in the four-photon state $|\psi_x^{(2,1)}\rangle \otimes |\phi_x^{(1,1,2)}\rangle \otimes |\phi_x^{(1,1,2,2)}\rangle$. The solid line shows the deposition rate for a four-photon absorption film. The dashed, dotted, and dash-dotted lines represent (normalized) the deposition rate for three-, two-, and one-photon absorption processes, respectively.

state $|\psi_x^{(4,3)}\rangle$. On the positive side, it is seen that if the film allows both for a three-photon and a four-photon absorption process, our method will still work, but it yields a somewhat poorer result than if the three-photon cross-section were identically zero. The ensuing deposition rate is moderately deteriorated as compared to the ideal case.

In Fig. 8 we have drawn similar curves for a six-mode, four-photon state that exposes pixel 7 (from the left) of 12 pixels. Each pixel is $\lambda/6$ wide, and the fundamental period of the deposition rate is 2λ. Again, three-, two-, and one-photon absorption processes will deteriorate the deposition rate, and in this case by a larger amount than for the two-mode state. The physical reason is that with a larger number of modes, there can also be a larger number of final states that will separate the interference paths into a larger number of distinguishable groups. This will primarily affect the (destructive) interference between the different absorption paths outside the deposition rate peak. However, in the six-mode case too, the deterioration is gradual. Hence, even if the three-photon cross section is not identically zero, the consequences are not catastrophic.

The final effect we wish to discuss regards the fact that the calculated deposition rate is an ensemble average. In an experiment, the actual deposition rate may look rather different than its expectation value. This effect has not been discussed in any of the previous papers on entangled-state subwavelength lithography [21–24]. If a state of the type given by Eq. (3.1) impinges on the film, the probability of state absorption is with all likelihood low. In addition, as has been discussed previously, each pixel defined on the film must contain many photosensitive grains since, for the method to make sense, the grains must be smaller (preferably much smaller) than the pixel size. Therefore, in order to expose a pixel, many exposure shots (per pixel) are needed. Since the absorption process is stochastic, the ensuing exposure will also be stochastic. The consequences of such an effect was studied in the context of the opposite process, namely image recognition, by Rose already in the 1940s [26,27] (an up-to-date review of this early work was recently written by Burgess [28]). In a first-order approximation, the exposure of each pixel can be modeled by a Poisson distribution with a mean determined by the relation between the absorption probability of a grain, the deposition rate at the pixel, and the exposure dose. It is clear that in order to have pixels with a relative variation in exposure of, say less than 10%, the mean number of exposed grains must be larger than 100. This in turn implies that the number of states that need to impinge on the film to expose this particular pixel must be much larger than 100. As a consequence, it is desirable that the state generator emits states with a high-repetition frequency in order to expose the film swiftly.

Finally, we wish to mention that the last, rather difficult, hurdle we have to deal with is how to generate two-mode reciprocal binomial states. For $N=2$, they can be prepared using standard parametric down conversion. Other schemes to produce them have been discussed in Ref. [29] and there is, at least, one realistic proposal for implementing these schemes for higher N [30].

V. CONCLUSIONS

We have developed a multimode extension of the subwavelength lithographic method based on multiphoton absorption proposed in Ref. [24]. We have shown the optimal way (in terms of the number of photons used in the process) to generate a pixellated pattern of given (subwavelength) resolution and pattern size. A salient feature of our proposal is that only one particular multimode photon number eigenstate needs to be prepared. Any pixellated pattern can be generated from this state by applying differential phase shifts between the modes. For a given lithographic feature resolution, the price to be paid for a larger pattern is that the complexity of the state used to expose the pattern increases. For

each doubling of the pattern area, two more modes in a one-photon state must be used. This also requires the film absorption process to increase by one, in terms of photons absorbed in the process. Therefore, it seems unlikely that it will be possible to make very large patterns.

We have also studied the effects of imperfections, in terms of losses, competing lower order multiphoton processes, and deposition-rate fluctuations due to the quantization of the light used for the exposure. We have shown that neither effect results in catastrophic consequences, demonstrating that the proposed method is somewhat robust against imperfections.

ACKNOWLEDGMENTS

This work was supported by the Swedish Research Council for Engineering Sciences (TFR), the Swedish Foundation for Strategic Research (SSF), and L M Ericssons stiftelse för främjande av elektroteknisk forskning.

[1] P.R. Dragsten, W.W. Webb, J.A. Paton, and R.R. Capranica, Science **185**, 55 (1974).
[2] A. Flock and D. Strelioff, Nature (London) **310**, 597 (1984).
[3] S. Kamimura, Appl. Opt. **26**, 3425 (1987).
[4] J. Jelles, B.J. Schnapp, and M.P. Scheetz, Nature (London) **331**, 450 (1988).
[5] W. Denk and W.W. Webb, Appl. Opt. **29**, 2382 (1990).
[6] C. Putman, B. De Grooth, N. Van Hulst, and J. Greve, J. Appl. Phys. **72**, 6 (1992).
[7] M.I. Kolobov and I.V. Sokolov, Phys. Lett. A **140**, 101 (1989).
[8] M.I. Kolobov and I.V. Sokolov, Zh. Éksp. Teor. Fiz. **96**, 1945, (1989) [Sov. Phys. JETP **69**, 1097 (1989)].
[9] M.I. Kolobov and I.V. Sokolov, Europhys. Lett. **15**, 271 (1991).
[10] M.I. Kolobov, Rev. Mod. Phys. **71**, 1539 (1999).
[11] M.I. Kolobov and C. Fabre, Phys. Rev. Lett. **85**, 3789 (2000).
[12] C. Fabre, J.B. Fouet, and A. Maître, Opt. Lett. **25**, 76 (2000).
[13] X. Min, L.-A. Wu, and H.J. Kimble, Phys. Rev. Lett. **59**, 278 (1987).
[14] J.J. Bollinger, W.M. Itano, D.J. Wineland, and D.J. Heinzen, Phys. Rev. A **54**, R4649 (1996).
[15] S.F. Huelga, C. Macchiavello, T. Pellizzari, A.K. Ekert, M.B. Plenio, and J.I. Cirac, Phys. Rev. Lett. **79**, 3865 (1997).
[16] V. Bužek, R. Derka, and S. Massar, Phys. Rev. Lett. **82**, 2207 (1999).
[17] J.G. Rarity and P.R. Tapster, Phys. Rev. A **41**, 5139 (1990).
[18] N. Margolus and L.B. Levitin, Physica D **120**, 188 (1998); J. Söderholm, G. Björk, T. Tsegaye, and A. Trifonov, Phys. Rev. A **59**, 1788 (1999).
[19] E.J.S. Fonseca, C.H. Monken, and S. Pádua, Phys. Rev. Lett. **82**, 2868 (1999).
[20] A. Trifonov, T. Tsegaye, G. Björk, J. Söderholm, E. Goobar, M. Atatüre, and A.V. Sergienko, J. Opt. B: Quantum Semiclassical Opt. **2**, 105 (2000).
[21] A.N. Boto, P. Kok, D.S. Abrams, S.L. Braunstein, C.P. Williams, and J.P. Dowling, Phys. Rev. Lett. **85**, 2733 (2000).
[22] G.S. Agarwal, R.W. Boyd, E.M. Nagasako, and S.J. Bentley, Phys. Rev. Lett. **86**, 1389 (2001).
[23] P. Kok, A.N. Boto, D.S. Abrams, C.P. Williams, S.L. Braunstein, and J.P. Dowling, Phys. Rev. A **63**, 063407 (2001).
[24] G. Björk, L.L. Sánchez Soto, and J. Söderholm, Phys.Rev. Lett. **86**, 4516 (2001).
[25] J. Jacobson, G. Björk, I. Chuang, and Y. Yamamoto, Phys. Rev. Lett. **74**, 4835 (1995).
[26] A. Rose, J. Soc. Motion Pict. Eng. **47**, 273 (1946).
[27] A. Rose, J. Opt. Soc. Am. **38**, 196 (1948).
[28] A.E. Burgess, J. Opt. Soc. Am. A **16**, 633 (1999).
[29] D.T. Pegg, S.M. Barnett, and L.S. Phillips, J. Mod. Opt. **44**, 2135 (1997).
[30] M.H.Y. Moussa and B.S.O. Baseia, Phys. Lett. A **238**, 223 (1998).